Journal of Alloys and Compounds 505 (2010) 727–732

Contents lists available at ScienceDirect

Journal of Alloys and Compounds

journal homepage: www.elsevier.com/locate/jallcom

Size controlled and morphology tuned fabrication of Fe_3O_4 nanocrystals and their magnetic properties

Shibing Ni[1], Xinghui Wang, Guo zhou, Feng Yang, Junming Wang, Qi Wang, Deyan He*

Department of Physics, Lanzhou University, Lanzhou 730000, PR China

ARTICLE INFO

Article history:
Received 25 June 2009
Received in revised form 20 June 2010
Accepted 22 June 2010
Available online 1 July 2010

Keywords:
Nanostructures
Crystal growth
Magnetic measurements

ABSTRACT

Size controlled and morphology tuned fabrication of Fe_3O_4 nanocrystals were achieved by a simple hydrothermal method using $(NH_4)_2Fe(SO_4)_2{\cdot}6H_2O$, hexamethylenetetramine, and sodium sulfate as original reaction materials. Fe_3O_4 particles with controlled size ranging from 160 nm to 2 μm were obtained by adding an appropriate amount of NH_4Ac to the reaction system. Fe_3O_4 quadrangular nanoplates with side length of about 500 nm were fabricated by adding optimum amount of urea. Box-like Fe_3O_4 nanocrystals were synthesized by adjusting the mol ratio between $(NH_4)_2Fe(SO_4)_2{\cdot}6H_2O$ and hexamethylenetetramine. The as-synthesized products were characterized by X-ray diffraction (XRD), field-emission scanning electron microscopy (FE-SEM), transmission electron microscopy (TEM), and selected area electron diffraction (SAED). Room-temperature magnetization curves that measured by vibrating sample magnetometer show morphology and size dependent magnetism.

1. Introduction

During the past few years, considerable researches have been done on the morphology and size controlled synthesis of micro- and nano-scale materials due to their unique chemical and physical properties that are relevant to their shape and size [1–4]. The design and synthesis of various magnetic architectural structures are of great interest and have actively been pursued due to their widely application such as pigmentation [5], recording materials [6], catalysts [7], ferrofluids [8], chemical sensors [9], and electro photographic developers [10].

Among all magnetic materials, magnetite (Fe_3O_4) has attracted much attention. It has not only been generally used as a very important ferromagnetic material for pigment, recording materials, catalysis, magnetocaloric refrigeration, printing ink, and magnetic resonance imaging, but also widely been considered as an ideal candidate for biological applications such as a tag for sensing and imaging [11,12], a drug-delivery carrier for antitumor therapy [13,14], an immunosensor for the detection of carcinoembryonic antigen in clinical immunoassay [15], and an activity agent for medical diagnostics [16] due to its good hydrophilic and biocompatible properties. Therefore, we are interested in developing simple method for size controlled and morphology tuned fabrication of Fe_3O_4 nanocrystals. For a long period of time, morphology controlled fabrication of nanomaterials was usually achieved by two ways: (i) adding surfactant [17]; (ii) adjusting the pH values by acid or alkali [18,19]. Since sulfates influenced fabrication of tungsten oxide nanocrystals with different morphologies was reported [20], soluble salts were testified to play important roles in the synthesis of nanomaterials in solution environment. Morphology controlled or well-dispersed nanomaterials were obtained by adding optimum amount of soluble salts [20,21]. In this paper, $(NH_4)_2Fe(SO_4)_2{\cdot}6H_2O$ and hexamethylenetetramine were used to synthesis of well-dispersed Fe_3O_4 nanocrystals in the presence of sodium sulfate. Ammonia acetate and urea were used to tune the size and morphologies of the products.

2. Experimental details

All the chemicals are analytical grade and purchased from Shanghai Chemical Reagents. In a typical procedure, 5 mmol $(NH_4)_2Fe(SO_4)_2{\cdot}6H_2O$, 2.5 mmol hexamethylenetetramine, and 0.5 g sodium sulfate were dissolved in 30 ml distilled water. For fabrication Fe_3O_4 particles with bigger size, different amount of NH_4Ac was added into the solution. Fe_3O_4 nanoplates were obtained by adding 0.3 g urea to the solution. After stirring for 20 min, the homogeneous green solution was transferred into a 50 ml Teflon lined autoclave, distilled water was subsequently added to 80% of its capacity. The autoclave was sealed and placed in an oven, heated at 90 °C for 24 h. After the reaction, the autoclave was cooled in air. The suspension was washed with distilled water and ethanol both four times at 6000 revolutions per minute for 5 min. The resulting black precipitates were finally dried in an oven at 60 °C for 24 h.

The structures of the resulting products were characterized by X-ray powder diffraction (Rigaku RINT2400 with Cu Kα radiation). Field-emission scanning electron microscopy (FE-SEM S-4800, Hitachi) and transmission electron microscopy (Hitachi, H-800) equipped with selected area electron diffraction (SAED) were employed for the morphologies, size and crystalline analysis. X-ray photoelectron spectroscopy (XPS) was performed on an Escalab MKII with Mg Kα ($h\nu$ = 1253.6 eV)

* Corresponding author: Fax: +86 931 8913554.
E-mail addresses: shibingni07@gmail.com (S. Ni), hedy@lzu.edu.cn (D. He).
[1] Present address: College of Mechanical and Material Engineering, Three Gorges University, 8 Daxue Road, Yichang 443002, PR China.

0925-8388/$ – see front matter © 2010 Elsevier B.V. All rights reserved.
doi:10.1016/j.jallcom.2010.06.126

as the exciting source at a pressure of 1.0×10^{-4} Pa and a resolution of 1.00 eV. The magnetic properties of the products were characterized by vibrating sample magnetometer (VSM, Lakeshore 7304, USA).

3. Results and discussion

Typical XRD patterns of the products synthesized by 5 mmol $(NH_4)_2Fe(SO_4)_2{\cdot}6H_2O$, 2.5 mmol hexamethylenetetramine, and 0.5 g Na_2SO_4 in the presence of different amount of NH_4Ac (a, 0 g; b, 0.1 g; c, 0.25 g; d, 0.5 g) and optimum amount of urea (e, 0.3 g) are shown in Fig. 1. The peaks of all samples can be indexed as face centered cubic Fe_3O_4 with lattice constant $a = 8.391$ Å, which are in good agreement with magnetite (JCPDS card No. 19-0629). No diffraction peaks other than those from Fe_3O_4 were obtained, indicating high purity of the as-synthesized products. The reactions during the hydrothermal process are likely to as follows:

$$(CH_2)_6N_4 + 10H_2O \rightarrow 6HCHO + 4OH^- + 4[NH_4]^+ \quad (1)$$

$$(NH_4)_2Fe(SO_4)_2{\cdot}6H_2O \rightarrow Fe^{2+} + 2[NH_4]^+ + 2(SO_4)^{2-} + 6H_2O \quad (2)$$

$$Fe^{2+} + 2OH^- \rightarrow Fe(OH)_2 \quad (3)$$

$$4Fe(OH)_2 + O_2 \rightarrow 4FeOOH + 2H_2O \quad (4)$$

$$Fe(OH)_2 + 2FeOOH + 4OH^- \rightarrow Fe_3O_4 + 4H_2O \quad (5)$$

The more mol ratio of hexamethylenetetramine, the high concentration of OH^- and NH_4^+ in the solution will be. High concentration of OH^- would ficilitate an Ostwald ripening growth, which is similar to that reported in literature [22]. In this Ostwald ripening process, the solid evacuation would start from the region underneath the surface layer and divide the pristine particle into two discrete parts, initiating the formation of box-like structure.

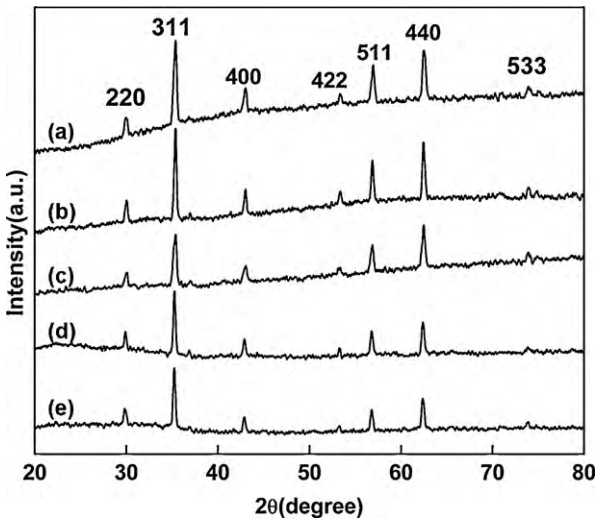

Fig. 1. XRD patterns of samples synthesized in the presence of (a) 0 g NH_4Ac; (b) 0.1 g NH_4Ac; (c) 0.25 g NH_4Ac; (d) 0.5 g NH_4Ac; (e) 0.3 g urea.

The effect of urea was likely as follows:

$$CO(NH_2)_2 + H_2O \rightarrow 2NH_3 + CO_2 \quad (6)$$

$$NH_3 + H_2O \rightarrow [NH_4]^+ + OH^- \quad (7)$$

The subsequent formation of Fe_3O_4 is the same as that described in expression (3)–(5).

The effect of NH_4Ac on particle size of Fe_3O_4 can be understood as follows: Ac^- would like to absorb on the surface of Fe_3O_4 nanocrystals due to its electronegative property. This will prevent particle agglomeration and facilitate the formation of Fe_3O_4 parti-

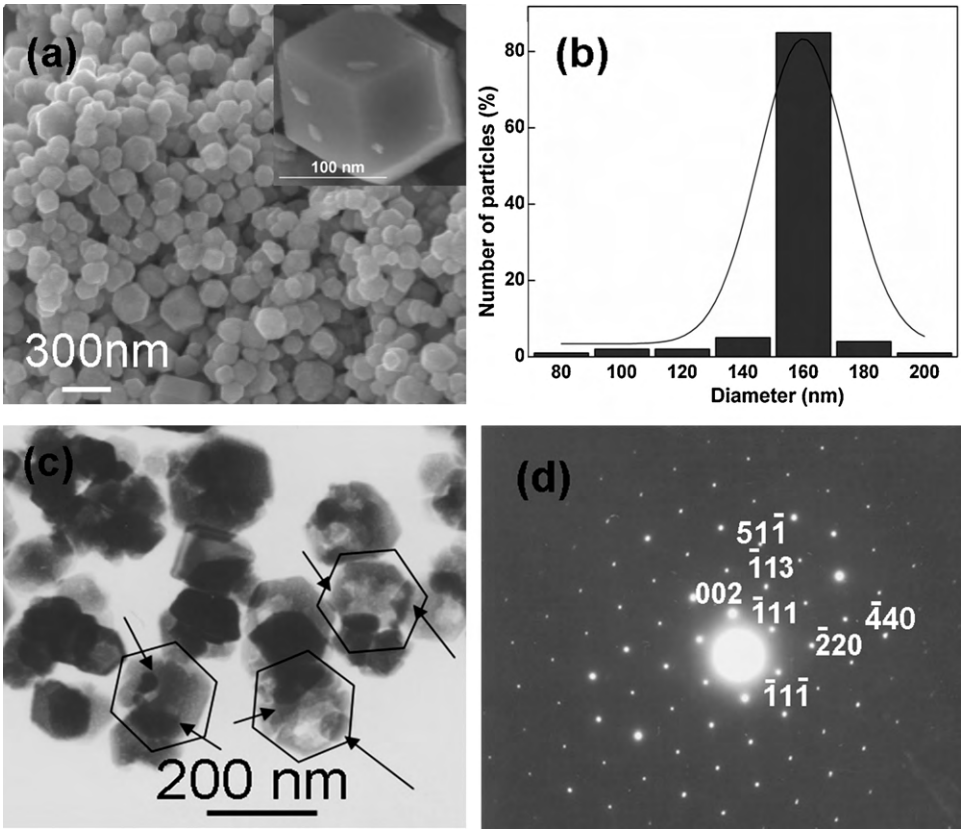

Fig. 2. (a) SEM image of Fe_3O_4 nanoparticles obtained without adding NH_4Ac and the size distribution (b); the insert of (a) is a SEM image of a single particle. (c) High magnification TEM image and (d) SAED pattern of Fe_3O_4 nanoparticles.

cles with bigger size via Ostwald ripening growth. In this process, larger crystallites are essentially immobile and keep growing while smaller ones are undergoing mass relocation through dissolving and regrowing.

Low magnification SEM image of Fe_3O_4 nanoparticles obtained from 5 mmol $(NH_4)_2Fe(SO_4)_2{\cdot}6H_2O$, 2.5 mmol hexamethylenetetramine, and 0.5 g Na_2SO_4 is shown in Fig. 2a. The insert of Fig. 2a is a SEM image of a single particle with well-developed surface, which exhibits quadrilateral facets. This morphology seems to be rhombic dodecahedra and in accordance with earlier report [23,24]. The obtained size of the particles was determined by analyzing the recorded SEM image. The estimated average size of those particles is 160 nm, whereas the particle size distribution is shown in histogram in Fig. 2b (fitted with Gaussian). A further elucidation of the geometrical morphology and size of the as-synthesized products is shown in a TEM image (Fig. 2c), which exhibits hexagonal morphology clearly. In agreement with above SEM findings, it is found in Fig. 2c that a single nanoparticle is about 80 nm in side length. Some of the hexagonal nanoparticles are not well developed, as it can be seen the accumulation of small particles with mean size of about 10 nm. The formation of single crystallized hexagonal nanoparticles is similar with that reported in literature [25]. Small particles are formed firstly and then followed by the aggregation of small particles to form big one. At last, big particles are fully grown to form single crystals. Furthermore, the highly crystalline nature of the as-synthesized products was confirmed by selected area electron diffraction measurement. Fig. 2d is a SAED pattern takes from Fig. 2c, which indicates single crystal structure and in accordance with the literature report [23].

XPS measurements provide further information for the evaluation of the composition and purity of the product obtained from 5 mmol $(NH_4)_2Fe(SO_4)_2{\cdot}6H_2O$, 2.5 mmol hexamethylenetetramine and 0.5 g sodium sulfate. The wide-scan XPS spectrum of the product is shown in Fig. 3a. The C 1s binding energy in the XPS spectrum is located at 289 eV, and it was standardized using C 1s as reference at 284.8 eV. All other peaks were calibrated accordingly. No obvious impurities can be detected. The two strong peaks at the Fe region of 724.8 and 711 eV are respectively assigned to Fe $2p_{1/2}$ and Fe $2p_{3/2}$, which is shown in Fig. 3b. Fig. 3c shows the high-resolution spectrum of O 1s, the low binding energy component centered at 530.4 eV can be attributed to O^{2-} oxidation state bound with Fe in the crystal lattice.

Fig. 4 shows TEM images of the samples fabricated by adding different amount of NH_4Ac to the reaction system. Fig. 4a presents a low magnification TEM image of the sample synthesized by adding 0.5 g NH_4Ac, indicating that the products consist of large quantity of microparticles. The mean side length of those particles is about 1 μm, which is much bigger than that of the products synthesized without adding NH_4Ac of about 80 nm. Moreover, hexagonal morphology of the particles is further observed through a magnified TEM image (Fig. 4b). Interestingly, when the quantity of NH_4Ac was regulated, the size of the products was as well tuned. Fig. 4c is a TEM image of the products obtained by adding 0.25 g NH_4Ac into the reaction system, which shows that the products are of hexagonal morphology with mean diameter of about 500 nm. The size of the as-synthesized particles continues to decrease when the quantity of NH_4Ac keeps on reducing. Fig. 4d is a TEM image of the products obtained by adding 0.1 g NH_4Ac, which indicates

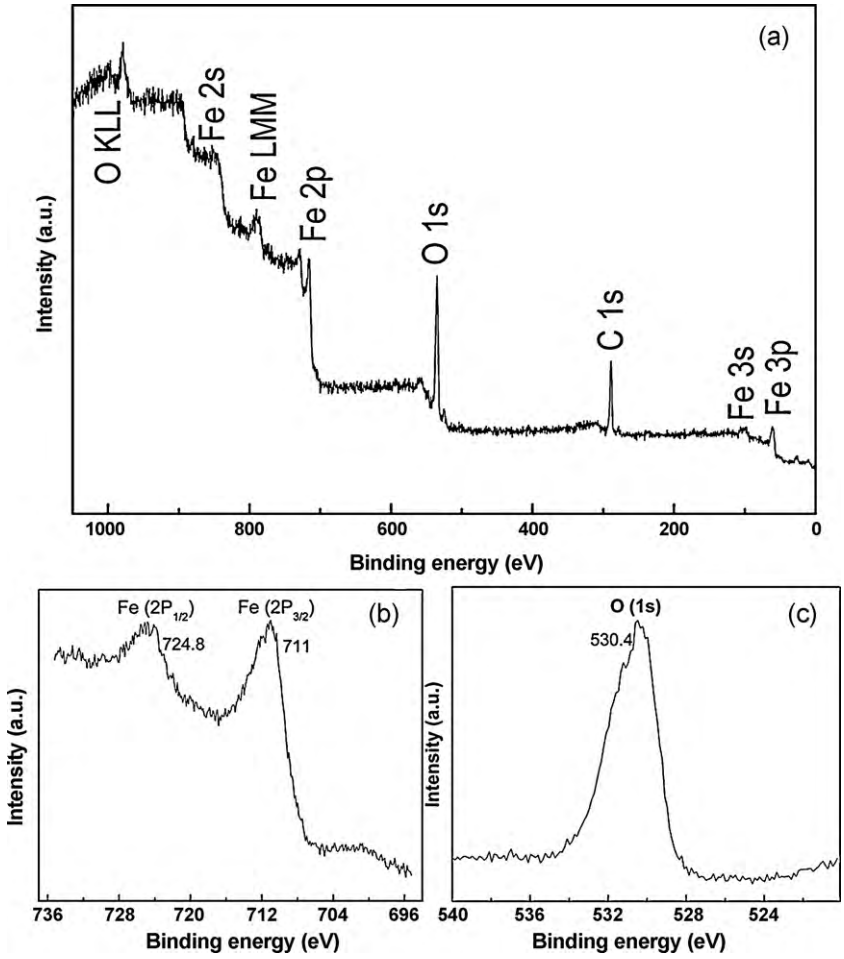

Fig. 3. XPS spectra of the as-prepared Fe_3O_4. (a) Wide-scan spectrum; (b) high-resolution spectrum for Fe 2p; (c) high-resolution spectrum for O 1s.

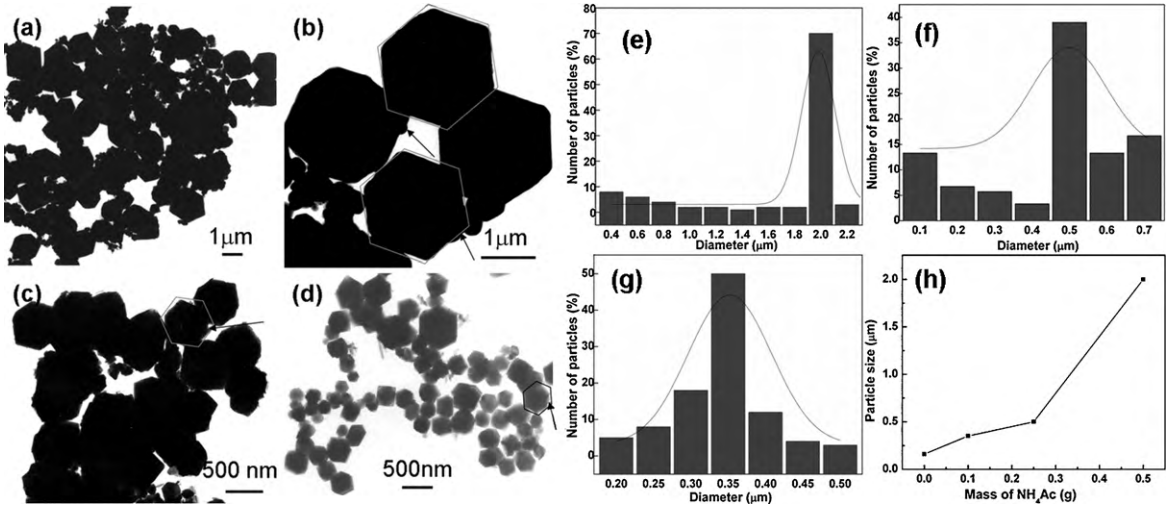

Fig. 4. TEM images of Fe_3O_4 nanoparticles obtained by adding different amount of NH_4Ac: (a) 0.5 g and its magnified TEM image (b); (c) 0.25 g; (d) 0.1 g; size distribution of the products obtained by adding different amount of NH_4Ac: (e) 0.5 g; (f) 0.25 g; (g) 0.1 g. (h) The variation of particle size versus adding amount of NH_4Ac.

that the mean diameter of those hexagonal nanoparticles is about 350 nm. The obtained size of those particles was determined by analyzing the recorded TEM images, whereas the size distributions of those particles are shown in histogram in Fig. 4e–g. (Fig. 4e, f, and g are corresponding to the histograms of the products shown in Fig. 4a, c, and d, respectively. Those curves are fitted with Gaussian.) Fig. 4 h is the variation of particle size as a function of adding amount of NH_4Ac. Fig. 5 shows the morphology of those products prepared with different amount of NH_4Ac. It is noticeable that the as-synthesized Fe_3O_4 particles are always of rhombic dodecahedra structure, though their size increases with added NH_4Ac [23,24]. The adding of NH_4Ac affected the solution environment, causing a mass relocation of small particles and formation of Fe_3O_4 particles with bigger size via Ostwald ripening growth. Moreover, the pH values do not obviously changed along with the adding amount of NH_4Ac due to its weak acidity.

It can be noticed that some little sized Fe_3O_4 nanoparticles formed along with the formation of bigger sized particles in the presence of NH_4Ac. This process of crystal growth and morphology evolution can be described as Ostwald ripening which involves the growth of large particles at the expense of the smaller ones driven by the tendency of the solid phase in the systems to adjust itself to achieve a minimum total surface free energy [26]. Regarding the growth progress, it is believed that NH_4Ac plays a crucial role in the formation of Fe_3O_4 nanoparticles with different size. As the origin of soluble salts affected growth is unclear, we propose coexistence and competition between NH_4^+ and Ac^- induce the Ostwald ripening growth.

Fig. 6a is a TEM image of the product obtained from 5 mmol $(NH_4)_2Fe(SO_4)_2{\cdot}6H_2O$, 0.5 g sodium sulfate, and 5 mmol hexamethylenetetramine, which presents a novel box-like morphology. The box-like morphology comes from the accumulation of small

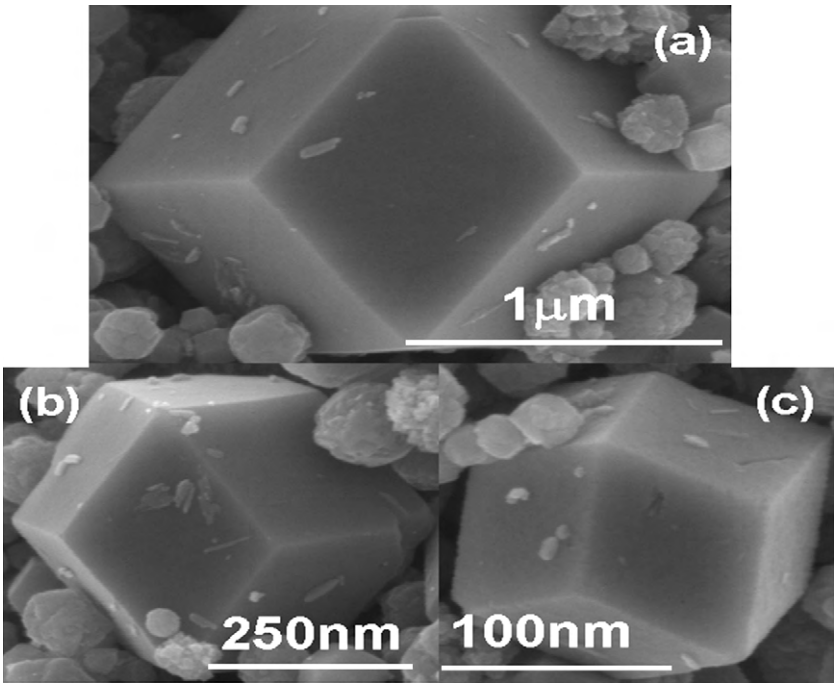

Fig. 5. SEM images of Fe_3O_4 particles prepared with different amount of NH_4Ac: (a) 0.5 g; (b) 0.25 g; (c) 0.1 g.

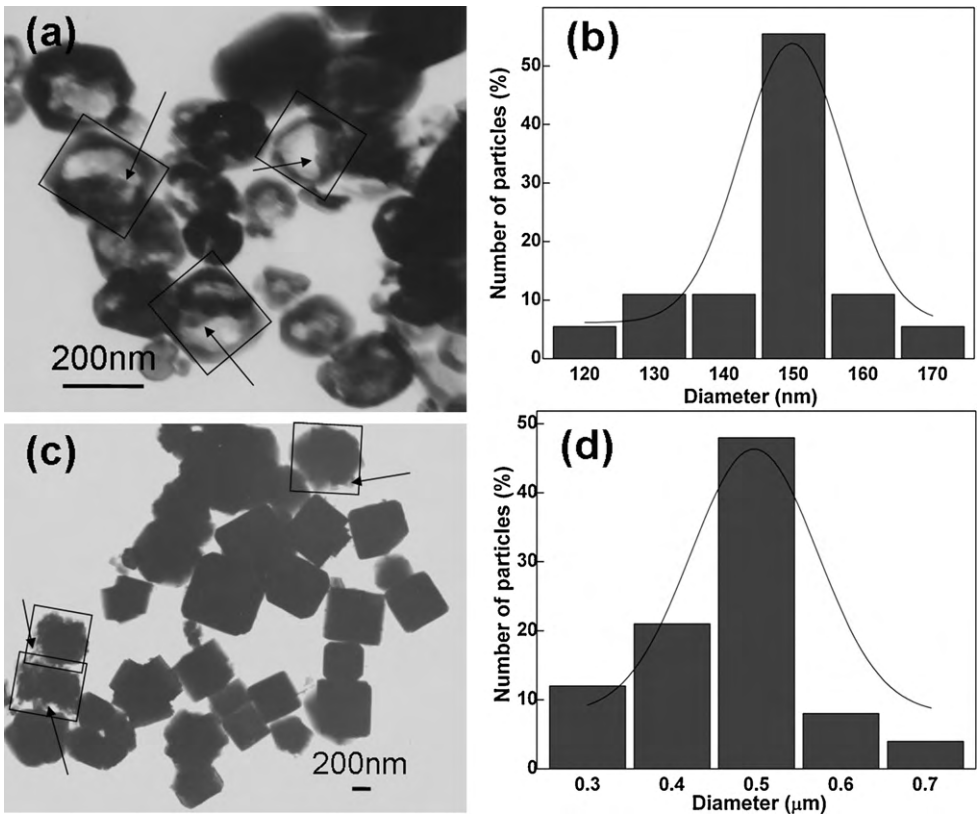

Fig. 6. (a) TEM image of nanoboxes obtained in optimum concentration of hexamethylenetetramine and the size distribution (b); (c) quadrangular nanoplates obtained by adding appropriate amount of urea and the size distribution (d).

particles and subsequent Ostwald ripening process (the arrows). The mean diameter and wall thickness of those nanoboxes are about 150 and 20 nm, respectively. No other new morphology was obtained when keeping on regulating the mole ratio between $(NH_4)_2Fe(SO_4)_2{\cdot}6H_2O$ and hexamethylenetetramine. The histogram of size distribution of nanoboxes in Fig. 6a is shown in Fig. 6b (the curve was fitted with Gaussian). It is interesting that the final products vary from hexagonal into quadrangle with bigger size when adding 0.3 g urea to the reaction system, which is shown in TEM image in Fig. 6c. It can be seen from the arrows that those quadrangle nanoplates are consist of lots of small particles. The obtained size of those nanoplates was determined by analyzing the recorded TEM image. The estimated average size of those nanoplates is 500 nm, whereas the particle size distribution is shown in histogram in Fig. 6d (the curve was fitted with Gaussian). On the basis of above experiment, it is obvious that hexamethylenetetramine and NH_4Ac play important roles in controlling the final morphology and size of the products, respectively. We propose special solution environments that are determined by ion species and concentration play crucial roles in the formation of Fe_3O_4 nanostructures. In addition, it is found experimentally that the morphology and size of the

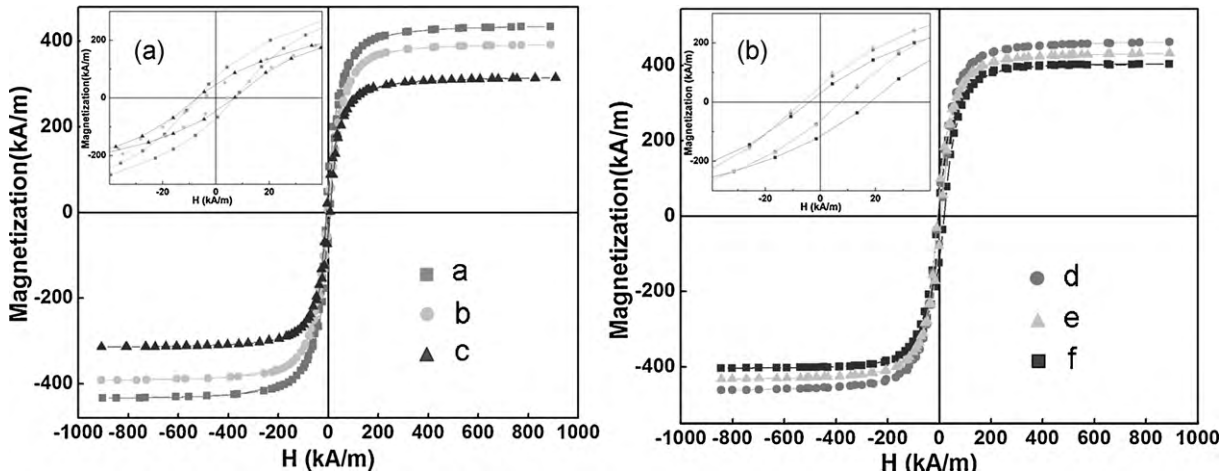

Fig. 7. Room-temperature magnetic hysteresis curves of morphology affected (a) quadrangle nanoplate (curve a), hexagonal nanoparticle (curve b), and nanobox (curve c) and size dependent (b) hexagonal nanoparticles with size 2 μm, 500 nm, and 350 nm (curve d, e, f); the insert are corresponding part hysteresis curves (field from −40 to 40 kA/m).

products do not change along with the increased reaction temperature.

Morphology and size dependent room-temperature magnetic hysteresis loops of those samples are shown in Fig. 7. It can be clearly seen from Fig. 7a that the saturation magnetization of quadrangle nanoplate (curve a), hexagonal nanoparticle (curve b), and nanobox (curve c) present degressive value. The saturation magnetization values were obtained by choosing an average value at the flat end of the curves, which are measured to be 434, 391, and 313.5 kA/m, respectively. They are lower than that of bulk Fe_3O_4 (440–518 kA/m), and in accordance with the size determined saturation magnetization report [27]. Furthermore, the insert part hysteresis curves reveal that their corresponding coercivity values are 6.99, 4.52, and 6.98 kA/m, which may probably be affected by their special morphologies. Different morphologies of Fe_3O_4 nanocrystals originate from different ways that small particles assemble, which may be affected by different solution environment. This assembly process can be testified from TEM images (the arrows in Fig. 2c, Fig. 6a and c).

Fig. 7b shows hysteresis curves of Fe_3O_4 nanoparticles with different size that were obtained by adding different amount of NH_4Ac (curve d (0.5 g), curve e (0.25 g), curve f (0.1 g)). As we know, the saturation magnetization of nanoparticles is lower than that of corresponding bulk sample and decreases with the reduction of particle size. It is found that the saturation magnetization values distinctly decrease along with the reduction of NH_4Ac, which may due to the size decreasing effect and are in accordance with above TEM images. The saturation magnetization values are 461.5, 433.5, and 403.5 kA/m while the mean diameter of the samples is 2 μm, 500 nm, and 350 nm, respectively. The coercivity values that can be seen from the insert part hysteresis curves are 11, 7.6, and 5.7 kA/m, which are lower than that of bulk Fe_3O_4 (9.2–12 kA/m). Different size of Fe_3O_4 originates from the assembly of small sized particles, which can be seen from TEM images (the arrows in Fig. 4b, c, and d).

4. Conclusions

In conclusion, well-dispersed Fe_3O_4 nanoparticles with controlled diameter from 160 nm to 2 μm, box-like morphology, and quadrangle nanoplates were synthesized by a simple hydrothermal method in the presence of sodium sulfate. We propose solution environments that determined by ion species and concentration play crucial roles in the dispersability and growth of magnetite. This soluble ion tuned synthesis will probably be widely adopted for size and morphology controlled fabrication in future. The effect of soluble ions in solution environment may be as much important as that of pH value or surfactant. Further work should be done to clarify the origin of the soluble salt affected synthesis.

Acknowledgements

We gratefully acknowledge the financial support from the Teaching and Research Award Program for Outstanding Young Teachers (MOE, China), Natural Science Foundation of China (NSFC, 50972075), key projects of Chinese Ministry of Education (D209083), and Education Office of Hubei Province (D20081304 and CXY2009A004). Moreover, the authors are grateful to Dr. Jianlin Li at Three Gorges University for his kind support to our research.

References

[1] C. Burda, X. Chen, R. Narayanan, M.A. El-Sayed, Chem. Rev. 105 (2005) 1025–1102.
[2] J.Y. Wang, F.L. Ren, R. Yi, A.G. Yan, G.Z. Qiu, X.H. Liu, J. Alloys Compd. 479 (2009) 791–796.
[3] Q.L. Li, C.B. Chang, H.X. Jing, Y.F. Wang, J. Alloys Compd. 495 (2010) 63–66.
[4] L.Y. Chen, H. Dai, Y.M. Shen, J.F. Bai, J. Alloys Compd. 491 (2010) L33–L38.
[5] X.Y. Wang, G.Q. Yang, Z.S. Zhang, L.M. Yan, J.H. Meng, Dyes Pigments 74 (2007) 269–272.
[6] B.M. Holmes, D.M. Newman, M.L. Wears, J. Magn. Magn. Mater. 315 (2007) 39–45.
[7] Y.G. Wang, J.W. Ren, X.H. Liu, Y.Q. Wang, Y. Guo, Y.L. Guo, G.Z. Lu, J. Colloid Interface Sci. 326 (2008) 158–165.
[8] R.Y. Hong, B. Feng, G. Liu, S. Wang, H.Z. Li, J.M. Ding, Y. Zheng, D.G. Wei, J. Alloys Compd. 476 (2009) 612–618.
[9] C. Ingrosso, M. Striccoli, A. Agostiano, E. Sardella, S. Keller, G. Blagoi, A. Boisen, M.L. Curri, Procedia Chem. 1 (2009) 32–35.
[10] P.E. Matijevic, in: L.L. Hench, D.B. Ulrich (Eds.), Colloid Science of Composites, System Science of Ceramic Chemical Processing, Wiley, New York, 1986, pp. 463–481.
[11] H. Lee, E. Lee, D.K. Kim, N.K. Jang, Y.Y. Jeong, S. Jon, J. Am. Chem. Soc. 128 (2006) 7383–7389.
[12] B. Fang, G.F. Wang, W.Z. Zhang, M.G. Li, X.W. Kan, Electroanalysis 17 (2005) 744–748.
[13] J. Dobson, Drug Dev. Res. 67 (2006) 55–60.
[14] C. Alexiou, R.J. Schmid, R. Jurgons, M. Kremer, G. Wanner, C. Bergemann, E. Huenges, T. Nawroth, W. Arnold, F.G. Parak, Eur. Biophys. J. Biophys. Lett. 35 (2006) 446–450.
[15] D.P. Tang, R. Yuan, Y.Q. Chai, J. Phys. Chem. B 110 (2006) 11640–11646.
[16] I. Koh, X. Wang, B. Varughese, L. Isaacs, S.H. Ehrman, D.S. English, J. Phys. Chem. B 110 (2006) 1553–1558.
[17] G.F. Zou, K. Xiong, C.L. Jiang, H. Li, T.W. Li, J. Du, Y.T. Qian, J. Phys. Chem. B 109 (2005) 18356–18360.
[18] X.L. Zhang, C.H. Sui, J. Gong, Z.M. Su, L.Y. Qu, J. Phys. Chem. C 111 (2007) 9049–9054.
[19] C. Jia, Y. Cheng, F. Bao, D.Q. Chen, Y.S. Wang, J. Cryst. Growth 294 (2006) 353–357.
[20] Z.J. Gu, T.Y. Zhai, B.F. Gao, X.H. Sheng, Y.B. Wang, H.B. Fu, Y. Ma, J.N. Yao, J. Phys. Chem. B 110 (2006) 23829–23836.
[21] Y. Sun, D.J. Riley, M.N.R. Ashfold, J. Phys. Chem. B 110 (2006) 15186–15192.
[22] B.P. Jia, L. Gao, J. Cryst. Growth 303 (2007) 616–621.
[23] F. Vereda, B. Rodríguez-González, J. Vicente, R. Hidalgo-Álvarez, J. Colloid Interface Sci. 318 (2008) 520–524.
[24] Q. Song, Y. Ding, Z.L. Wang, Z.J. Zhang, J. Phys. Chem. B 110 (2006) 25547–25550.
[25] T. Sugimoto, E. Matijević, J. Colloid Interface Sci. 74 (1980) 227–243.
[26] C.Q. Hu, Z.H. Gao, X.R. Yang, Chem. Phys. Lett. 429 (2006) 513–517.
[27] D.B. Yu, X.Q. Sun, J.W. Zou, Z.R. Wang, F. Wang, K. Tang, J. Phys. Chem. B 110 (2006) 21667–21671.